Hard x-ray photoelectron spectroscopy investigation of annealing effects on buried oxide in GaAs/Si junctions by surface-activated bonding

Shoji Yamajo[a], Sanji Yoon[a], Jianbo Liang[a], Hassanet Sodabanlu[b], Kentaro Watanabe[b], Masakazu Sugiyama[b], Akira Yasui[c], Eiji Ikenaga[c], and Naoteru Shigekawa[a,*]

[a]Graduate School of Engineering, Osaka City University, Osaka 558-8585, Japan

[b]School of Engineering, the University of Tokyo, Bunkyo-ku, Tokyo 113-0032, Japan

[c]Japan Synchrotron Radiation Research Institute (JASRI/SPring-8), Sayo, Hyogo 679-5198, Japan

Hard x-ray photoelectron spectroscopy measurements are performed on ≈10-nm-thick GaAs film/Si substrate junctions fabricated by the surface activated bonding and selective wet etching. The chemical shifts of Ga-O and As-O signals in Ga $2p_{3/2}$ and As $2p_{3/2}$ core spectra indicate that oxides are formed in a part of GaAs films neighboring GaAs/Si interfaces due to the surface activation process. Analyses of Ga-O and As-O signals show that the thickness of such buried oxides is decreased due to a post-bonding annealing at temperatures up to 400 °C. This means that the electrical properties of bonding interfaces, which are in the meta-stable states, are improved by the annealing. The thickness of oxides is different from that of amorphous-like transition layers at the GaAs/Si interfaces observed by transmission electron microscopy.

Keywords:

GaAs/Si; surface activated bonding; HAXPES; buried interface

*E-mail address: shigekawa@eng.osaka-cu.ac.jp

1. *Introduction*

III-V semiconductor/Si junctions have a potential for fabricating novel functional devices such as tandem solar cells [1,2], bipolar transistors [3], and high electron mobility transistors [4]. However, defects and dislocations with high densities are typically introduced in III-V layers grown on Si substrates due to the large difference in lattice constants and thermal expansion coefficients [5,6]. One way to overcome these difficulties is usage of the surface-activated bonding (SAB) method, in which the surfaces of the bonded substrates are irradiated by a fast atom beam (FAB) of Ar, i.e. the surfaces are activated, prior to the bonding [7,8]. SAB-based interfaces have been successfully applied for fabricating III-V/Si hybrid tandem solar cells that target both high efficiency and low costs [8,9].

The electrical properties of various SAB-based heterojunctions such as Si/GaAs, Si/InP, and Ge/Ge junctions were reported [10-13]. We previously suggested that the electrical properties in SAB-based Si/GaAs, Si/SiC and GaAs/GaN interfaces were strongly influenced by interface states formed during the surface activation process [14-16]. We also found that the resistance across n^+-GaAs/n^+-Si interfaces was lowered by annealing the interfaces [17].

Nanometer-scale structures, or nanostructures, of bonding interfaces have been examined using a transmission electron microscope (TEM). It was reported that amorphous-like transition layers were formed at the bonding interfaces [18,19]. The chemical properties, or properties of atomic bonds, of interfaces, however, have not yet been fully understood although the electrical properties of interfaces are likely to be strongly influenced by their chemical properties.

The chemical properties of interfaces formed several nm or several-tens nm below surfaces, or buried interfaces, have been investigated using a hard x-ray photoelectron spectroscopy (HAXPES), in which x-ray photoelectron spectroscopy (XPS) signals are measured using an incident x-ray with photon energies of several keV [20]. The properties of various types of buried interfaces such as SiO_2/Si, Al_2O_3/Si, and $InGaZnO_4$/Si have been examined using HAXPES [21-23]. In most cases, HAXPES have been applied for interfaces prepared by epitaxially growing [24] or depositing thin films on substrates [25].

In this work, we prepared GaAs/Si interfaces by means of SAB and the subsequent annealing. We performed HAXPES measurements of the interfaces with emphasis on Ga $2p_{3/2}$ and As $2p_{3/2}$ core spectra. XPS signals due to Ga-O and As-O bonds were analyzed so that the thickness of oxides in GaAs films in the vicinity of bonding interfaces was estimated. We also performed their TEM observation and estimated

the thickness of the transition layers at the interfaces. The thickness of the oxides and that of the transition layers were compared with each other.

2. Experimental

We prepared a GaAs/InGaP epitaxial substrate, which was composed of a 240-nm-thick InGaP etch-stopper and a 10-nm-thick undoped GaAs grown on a GaAs (100) substrate. The epitaxial substrate was bonded to an n-type Si (100) substrate with a carrier concentration of 4.8×10^{16} cm^{-3} using SAB. The substrates were not heated during the bonding process. After bonding, samples were annealed at different temperatures (200, 300, and 400 °C) for 1 min in a N_2 gas ambient. Then the GaAs substrate and InGaP etch stopper were successively removed by selective wet etching so that ≈10-nm-thick undoped GaAs film/Si substrate junctions were obtained. We also prepared an unprocessed GaAs (100) substrate and a GaAs substrate with the surface irradiated by an Ar FAB for the same condition as employed in the SAB process. All samples were diced into 2 mm by 5 mm pieces.

HAXPES measurements were carried out using BL47XU at SPring-8 with a take-off angle of 40°. The excitation X-ray beam used for HAXPES was monochromatized with Si (111) double crystal and Si (444) channel-cut monochromators, which provides a 7940-eV X-ray with a bandwidth of ~40 meV, a focal spot size of 30 μm (horizontal)·40 μm (vertical), and a photon flux of 2.8×10^{11} photons/s. A VG Scienta R4000 hemisphere electron analyzer was used. The binding energies of the HAXPES spectra were calibrated using the Fermi energy of an Au reference. Photoelectron signals due to Ga $2p_{3/2}$ and As $2p_{3/2}$ core levels were mainly examined. We also investigated the bonding interfaces of the GaAs/Si junctions before annealing and after annealing at 300 and 400 °C using TEM with 200-keV incident electron beams. The samples for TEM observations were fabricated by a micro-sampling method using a focused ion beam (FIB) of Ga species.

3. Results

Cross sectional TEM images of the GaAs/Si bonding interface before annealing and those after annealing at 300 and 400 °C are shown in Figs. 1(a), 1(b) and 1(c), respectively. No dislocations were observed at bonding interfaces irrespective of the annealing temperature. A 4-nm-thick amorphous-like transition layer, which was attributed to a damage caused by irradiation of Ar FAB, was observed at the interface without annealing. The transition layer was partly recrystallized and slightly thinned (~2.5 nm thick) due to the 300 °C annealing. It disappeared when the junction was annealed at 400 °C. Similar behaviors were

observed at the Si/Si and 4H-SiC/Si bonding interface fabricated by SAB [26,27].

Ga $2p_{3/2}$ core spectra in HAXPES of GaAs/Si junctions before annealing and after annealing at 200, 300, and 400 °C are shown in Figs. 2(a)-2(d), respectively. A Ga $2p_{3/2}$ core spectrum of a surface of an unprocessed GaAs substrate is given in Fig. 2(e). That of an irradiated GaAs surface is shown in Fig. 2(f). The respective core spectra were separated into two components at binding energies of ≈1117.1 and ≈1118.1 eV. The peaks at ≈1117.1 and ≈1118.1 eV were attributed to Ga-As and Ga-O bonds, respectively, by comparing observed binding energies with a literature [28]. The binding energies and intensities of the respective components were estimated by a least-squares fitting to a Voigt (convoluted Lorentzian with Gaussian) function [23,29]. The background was subtracted using Shirley method [30]. Curves obtained by fitting were in good agreement with the experimental data as is shown in the respective figures. The estimated binding energies of Ga-As and Ga-O peaks, their full widths at half maximum (FWHM) as well as the Ga-O intensity normalized to the Ga-As intensity (Ga-O/Ga-As) are summarized in Table I.

As $2p_{3/2}$ core spectra of GaAs/Si junctions before annealing and after annealing at 200, 300, and 400 °C are shown in Figs. 3(a)-3(d), respectively. As $2p_{3/2}$ core spectra of unprocessed and irradiated GaAs surfaces are shown in Figs. 3(e) and 3(f). Similarly to the case of Ga $2p_{3/2}$ core spectra, the respective As $2p_{3/2}$ core spectra were separated into two components. The peaks at ≈1322.7 and ≈1325.8 eV were attributed to As-Ga and As-O bonds, respectively. The binding energies and intensities of the respective components were estimated using a similar method to the process for treating Ga $2p_{3/2}$ core spectra. The results of fittings are also shown in the respective figures. The binding energies and FWHM of As-Ga and As-O peaks as well as the normalized As-O intensity (As-O/As-Ga) are given in Table I. We found that the normalized Ga-O and As-O intensities of GaAs substrates were increased due to the Ar-beam irradiation. In contrast, the normalized intensities of GaAs/Si junctions were decreased by increasing the annealing temperature.

4. Discussion

The Ga-O peak appeared at a chemical shift of ≈0.7 eV higher binding energy in the unprocessed surface of GaAs substrate. The chemical shift was increased to ≈1.2 eV by irradiating the surface by Ar FAB. The 0.7 and 1.2 eV chemical shifts are attributed to Ga_2O and GaO compounds, respectively [31]. Consequently, the change in chemical shifts suggests that the oxidation of Ga species is advanced ($Ga_2O \rightarrow GaO$) [32] by irradiating a GaAs surface by an Ar FAB. The chemical shifts of Ga-O peaks observed for GaAs/Si

junctions (≈1.5 eV) were close to that for an irradiated GaAs surface, which suggests that XPS signals come from oxides in GaAs neighboring the bonding interfaces, or buried oxide layers. The chemical shifts of the As-O peaks were 3.1-3.4 eV in all samples. The As-O peaks observed for all samples are, then, likely to be due to AsO compounds [31]. The binding energies of Ga-As and As-Ga peaks in the bonding interface were higher than that of GaAs substrate by 0.2-0.4 eV. The difference in binding energies between GaAs/Si interfaces and GaAs substrates was probably due to the difference in pinning of Fermi levels.

We estimated the thickness of oxides on surfaces of GaAs substrates from the normalized Ga-O and As-O intensities by using a method reported in literatures [28,32,33]. The oxides were assumed to be represented by GaO_x (AsO_x) compounds in handling Ga (As) $2p_{3/2}$ signals. The ratio of intensities of XPS signals coming from the native oxide and GaAs substrate (I_o and I_{GaAs}) are expressed by

$$\frac{I_o}{I_{GaAs}} = \frac{n_o\lambda_o\left\{1-exp\left(-\frac{d_o}{\lambda_o \sin\theta}\right)\right\}}{n_{GaAs}\lambda_{GaAs}exp\left(-\frac{d_o}{\lambda_o \sin\theta}\right)}, \quad (1)$$

where n_o and n_{GaAs} are the atomic density of oxides and GaAs [37], λ_o and λ_{GaAs} are the mean free path of photoelectrons of oxides and GaAs, d_o is the thickness of oxides, and θ is the take-off angle, respectively. Equation (1) gives

$$d_o = \lambda_o \sin\theta \, ln\left(\frac{n_{GaAs}\lambda_{GaAs}I_o}{n_o\lambda_o I_{GaAs}} + 1\right). \quad (2)$$

Using the method proposed by Tanuma, Powell, and Penn [38], the mean free path was estimated to be 8.31, 9.74, 10.31, and 10.58 nm for the Ga-O, As-O, As-Ga, and Ga-As signals, respectively. The atomic densities of GaO_x and AsO_x compounds as well as GaAs were 5.88, 3.74, and 5.31 g/cm^3. By using eq. (2) for the normalized Ga-O and As-O intensities for the unprocessed surface of GaAs substrate, the thicknesses of GaO_x and AsO_x compounds were estimated to be 0.58 and 0.22 nm respectively, which provides a measure for the thickness of native oxides on such a surface.

We assumed that GaAs films bonded to Si substrates were composed of native oxides, GaAs layers, and buried oxides from the top to the bottom. The thickness of the buried oxides was estimated using a process similar to that applied for GaAs substrates. The intensity ratio of oxide-based peaks to the main peaks in the bonding samples can be expressed as

$$\frac{I_o}{I_{GaAs}} = \frac{n_o\lambda_o\left\{1-\exp\left(-\frac{d_o}{\lambda_o \sin\theta}\right)+\exp\left(-\frac{d_o}{\lambda_o \sin\theta}\right)\exp\left(-\frac{D-d_{bur}-d_o}{\lambda_{GaAs}\sin\theta}\right)\left(1-\exp\left(-\frac{d_{bur}}{\lambda_o \sin\theta}\right)\right)\right\}}{n_{GaAs}\lambda_{GaAs}\exp\left(-\frac{d_o}{\lambda_o \sin\theta}\right)\left(1-\exp\left(-\frac{D-d_{bur}-d_o}{\lambda_{GaAs}\sin\theta}\right)\right)}, \quad (3)$$

where D and d_{bur} are the thicknesses of GaAs films and buried oxides, respectively. The thicknesses of buried oxides for the respective annealing temperatures were obtained by solving the Eq. (3) numerically.

The relationship between d_{bur} and the annealing temperature is shown in Fig. 4. We find that d_{bur} for the interface without annealing, 8.4 and 7.4 nm on the Ga-O and As-O signals, respectively, is much larger

1 than the aforementioned d_o. We also find that d_{bur} gradually decreases due to the annealing, which is in
2 contrast with a report indicating that the oxide on surface of GaAs substrate got thicker as the substrate
3 was annealed at higher temperatures in vacuum [34]. The change in d_{bur} due to the annealing is likely to
4 be related to the improvement of the electrical conduction across n-Si/n-GaAs interfaces [17]. The
5 thickness of buried oxides based on the Ga-O signal was close to that based on the As-O signal at the
6 respective annealing temperatures up to 300 °C. However, at 400 °C, d_{bur} based on the As-O signal was
7 smaller than that based on the Ga-O signal, which was hypothetically explained by selective dissolution
8 and evaporation of AsO_x and subsequent formation of Ga-rich layer.

9 The native oxides on a surface of a GaAs substrate were reportedly dissolved and evaporated when the
10 substrate temperature was as high as 500 or 600 °C [35,36]. The observed decrease in d_{bur} at lower
11 temperatures suggests that the bonding interfaces are in the metastable state. The interfaces free from the
12 oxide layers could be achieved so that the interface resistances should be further lowered by optimizing
13 the post-bonding annealing process.

14 We note that the thickness of the transition layers achieved by TEM observation is smaller than d_{bur}. One
15 possible explanation for this disagreement is that the transition layers might be recrystallized and got
16 thinner due to the unintentional heating while the samples for TEM observation were prepared using FIB.

17 5. Conclusions

18 We fabricated ≈10-nm-thick GaAs/Si substrate junctions by using surface-activated bonding of a
19 GaAs/InGaP heterostructure grown on a GaAs (100) substrate to a Si (100) substrate and selective wet
20 etching of the GaAs substrate and InGaP layer. We annealed the junctions at different temperatures
21 between 200 and 400 °C. We performed hard x-ray photoelectron spectroscopy (HAXPES) measurements
22 of junctions and GaAs substrates and examined contributions of Ga-O and As-O bonds. The chemical
23 shifts of Ga-O and As-O peaks indicated that oxide composed of GaO and AsO compounds were formed
24 in junctions similarly to oxides on surfaces of GaAs substrates irradiated by Ar beams. This suggested that
25 the oxides observed for GaAs/Si junctions were due to the Ar beam irradiation and were regarded as buried
26 oxides that were distributed in the vicinity of GaAs/Si interfaces. Furthermore, the thickness of the buried
27 oxides was decreased from ≈ 8 to ≈ 5.6 nm by annealing junctions at 400 °C, which meant that the
28 interfaces were in the meta-stable states. The decrease in thickness of buried oxide was related to the
29 improvement of the electrical properties of interfaces by such an annealing. The thickness of oxides

1 disagreed with that of amorphous-like transition layers found by TEM observation, which might be related
2 to the possible recrystallization of the GaAs/Si interfaces during the preparation of TEM samples. The
3 abrupt decrease in As-O signals observed after the 400-℃ annealing might be due to the dissolution and
4 evaporation of As-O bonds.
5
6 Acknowledgement—This work was supported by the “Research and Development of ultra-high efficiency
7 and low-cost III-V compound semiconductor solar cell modules (High efficiency and low-cost III-V/Si
8 tandem)” project of New Energy and Industrial Technology Development Organization (NEDO).
9
10

References

[1] T. Soga, T. Kato, K. Baskar, C. L. Shao, T. Jimbo, M. Umeno, J. Crystal Growth 170 (1997) 447-450.

[2] T. Soga, K. Baskar, T. Kato, T. Jimbo, M. Umeno, J. Crystal Growth 174 (1997) 579-584.

[3] R. Fischer, N. Chand, W. Kopp, H. Morkoç, L. P. Erickson, R. Youngman, Appl. Phys. Lett. 47 (1985) 397-399.

[4] M. Marso, M. Wolter, P. Javorka, P. Kordoš, H. Lüth, Appl. Phys. Lett. 82 (2003) 633-635.

[5] R. Hull, A. Fischer-Colbrie, S. J. Rosner, S. M. Koch, J. S. Harris, Appl. Phys. Lett. 51 (1987) 1723-1725.

[6] M. Yamaguchi, M. Tachikawa, Y. Itoh, M. Sugo, S. Kondo, J. Appl. Phys. 68 (1990) 4518-4522.

[7] H. Takagi, K. Kikuchi, R. Maeda, T. R. Chung, T. Suga, Appl. Phys. Lett. 68 (1996) 2222-2224.

[8] N. Shigekawa, J. Liang, R. Onitsuka, T. Agui, H. Juso, T. Takamoto, Jpn. J. Appl. Phys. 54 (2015) 08KE03-1 - 08KE03-5.

[9] S. Essig, J. Benick, M. Schachtner, A. Wekkeli, M. Hermle, F. Dimroth, IEEE J. Photovoltaics 5 (2015) 977-981.

[10] S. Essig, O. Moutanabbir, A. Wekkeli, H. Nahme, E. Oliva, A. W. Bett, F. Dimroth, J. Appl. Phys. 113 (2013) 203512-1 - 203512-6.

[11] M. M. R. Howlader, T. Watanabe, T. Suga, J. Vac. Sci. Technol. B 19 (2001) 2114-2118.

[12] M. M. R. Howlader, T. Watanabe, T. Suga, J. Appl. Phys. 91 (2002) 3062-3066.

[13] E. Higurashi, Y. Sasaki, R. Kurayama, T. Suga, Y. Doi, Y. Sawayama, I. Hosako, Jpn. J. Appl. Phys. 54 (2015) 030213-1 - 030213-7.

[14] J. Liang, T. Miyazaki, M. Morimoto, S. Nishida, N. Watanabe, N. Shigekawa, Appl. Phys. Express 6 (2013) 021801-1 - 021801-3.

[15] J. Liang, S. Nishida, T. Hayashi, M. Arai, N. Shigekawa, Appl. Phys. Lett. 105 (2014) 151607-1 - 151607-4.

[16] S. Yamajo, J. Liang, N. Shigekawa, Jpn. J. Appl. Phys. 57 (2018) 02BE02-1 - 02BE02-5.

[17] J. Liang, L. Chai, S. Nishida, M. Morimoto, N. Shigekawa, Jpn. J. Appl. Phys. 54 (2015) 030211-1 - 030211-5.

[18] H. Takagi, R. Maeda, N. Hosoda, T. Suga, Jpn. J. Appl. Phys. 38 (1999) 1589-1594.

[19] M. Sakata, T. Oyake, J. Maire, M. Nomura, E. Higurashi, J. Shiomi, Appl. Phys. Lett. 106 (2015)

081603-1 - 081603-4.

[20] S. Toyoda, M. Oshima, J. Appl. Phys. 120 (2016) 085306-1 - 085306-10.

[21] L. A. Walsh, G. Hughes, P. K. Hurley, J. Lin, J. C. Woicik, Appl. Phys. Lett. 101 (2012) 241602-1 - 241602-4.

[22] J. R. Church, C. Weiland, R. L. Opila, Appl. Phys. Lett. 106 (2015) 171601-1 - 171601-4.

[23] K. Lee, K. Nomura, H. Yanagi, T. Kamiya, E. Ikenaga, T. Sugiyama, K. Kobayashi, H. Hosono, J. Appl. Phys. 112 (2012) 033713-1 - 033713-6.

[24] S. Heun, M. Sugiyama, S. Maeyama, Y. Watanabe, K. Wada, M. Oshima, Phys. Rev. B 53 (1996) 13534-13541.

[25] K. Nomura, T. Kamiya, E. Ikenaga, H. Yanagi, K. Kobayashi, H. Hosono, J. Appl. Phys. 109 (2011) 073726-1 - 073726-8.

[26] M. Morimoto, J. Liang, S. Nishida, N. Shigekawa, Jpn. J. Appl. Phys. 54 (2015) 030212-1 - 030212-5.

[27] J. Liang, S. Nishida, M. Arai, N. Shigekawa, Appl. Phys. Lett. 104 (2014) 161604-1 - 161604-4.

[28] M. Paul, A. Müller, A. Ruff, B. Schmid, G. Berner, M. Mertin, M. Sing, R. Claessen, Phys. Rev. B 79 (2009) 233101-1 - 233101-4.

[29] T. N. Bhat, M. Kumar, M. K. Rajpalke, B. Roul, S. B. Krupanidhi, N. Sinha, J. Appl. Phys. 109 (2011) 123707-1 - 123707-5.

[30] D. A. Shirley, Phys. Rev. B 5 (1972) 4709-4714.

[31] J. Ivanco, T. Kubota, H. Kobayashi, J. Appl. Phys. 97 (2005) 073712-1 - 073712-7.

[32] T. Ishikawa, H. Ikoma, Jpn. J. Appl. Phys. 31 (1992) 3981-3987.

[33] Z. Liu, Y. Sun, F. Machuca, P. Pianetta, W. E. Spicer, R. F.W. Pease, J. Vac. Sci. Technol. A 21 (2003) 212-218.

[34] H. Morota, S. Adachi, J. Appl. Phys. 105 (2009) 043508-1 - 043508-7.

[35] L. H. Li, E. H. Linfield, R. Sharma, A. G. Davies, Appl. Phys. Lett. 99 (2011) 061910-1 - 061910-3.

[36] R. P. Vasquez, B. F. Lewis, F. J. Grunthaner, Appl. Phys. Lett. 42, (1983) 293-295.

[37] Pradyot Patnaik, Handbook of Inorganic Chemicals, McGraw-Hill Professional, New York, 2002.

[38] S. Tanuma, C. J. Powell, and D. R. Penn, Surf. Interf. Anal. 21, (1994) 165-176.

Figure captions

Fig. 1. Cross-sectional TEM images of the GaAs/Si interface (a) without and with annealing at (b) 300 and (c) 400 ℃.

Fig. 2. Ga $2p_{3/2}$ core spectra of the GaAs/Si interface (a) without and with annealing at (b) 200, (c) 300, and (d) 400 ℃ and Ga $2p_{3/2}$ core spectra of (e) the unprocessed surface of GaAs substrate and (f) the surface irradiated by Ar beams

Fig. 3. As $2p_{3/2}$ core spectra of the GaAs/Si interface (a) without and with annealing at (b) 200, (c) 300, and (d) 400 ℃ and As $2p_{3/2}$ core spectra of (e) the unprocessed surface of GaAs substrate and (f) the surface irradiated by Ar beams.

Fig. 4. The dependencies of thicknesses of buried oxides of GaAs/Si interfaces on annealing temperature. The thicknesses of native oxides on an unprocessed GaAs substrate are also shown.

Table captions

Table I. The estimated binding energy of each peak. FWHM and normalized intensities of Ga-O and As-O signals of respective samples are also shown.

1

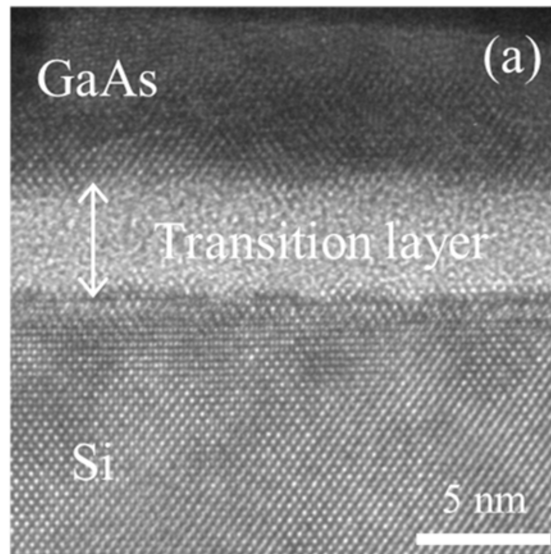

2

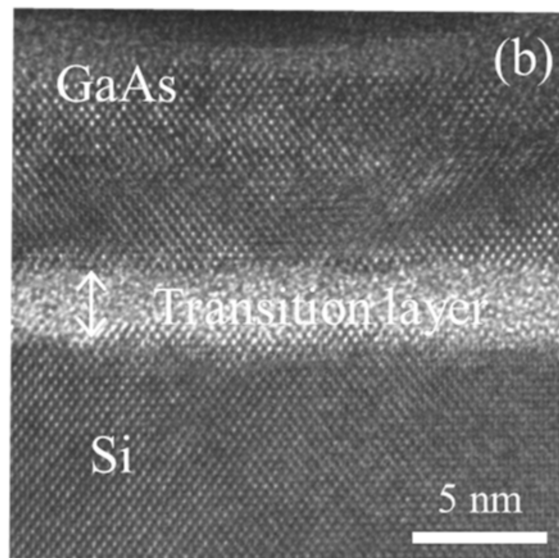

3

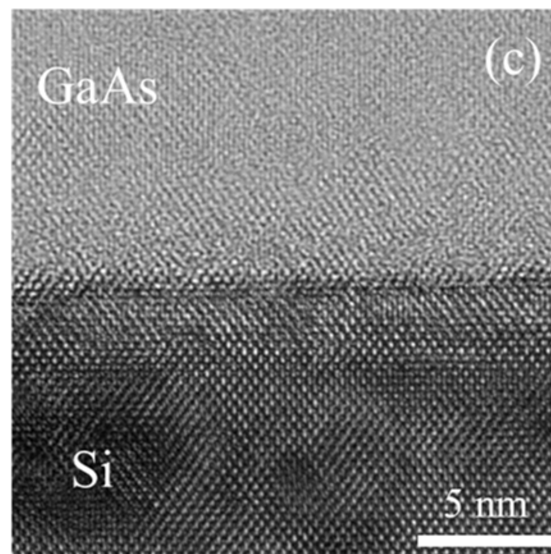

4

5

6 Fig. 1(a), 1(b) and 1(c).

1
2
3
4
5
6
7
8
9
10
11
12
13
14
15
16
17
18
19
20
21
22
23
24
25
26
27
28
29
30
31
32
33
34
35
36
37
38
39

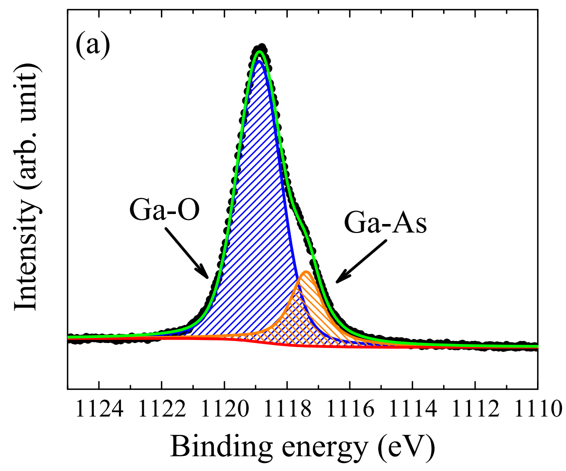

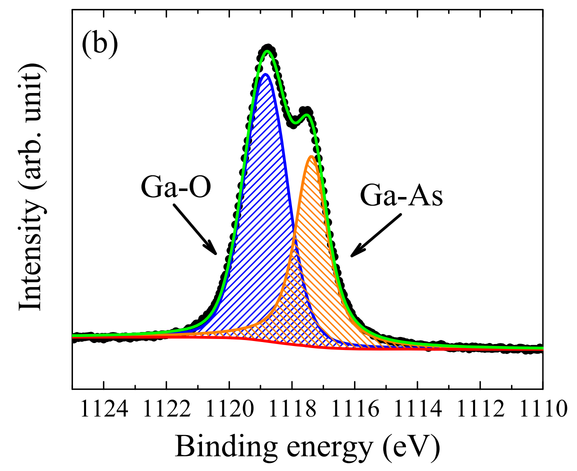

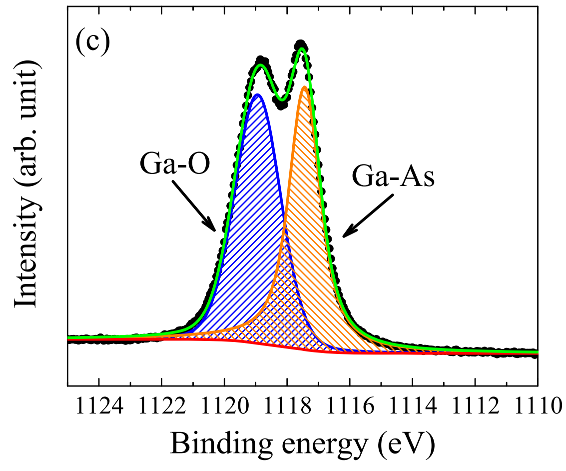

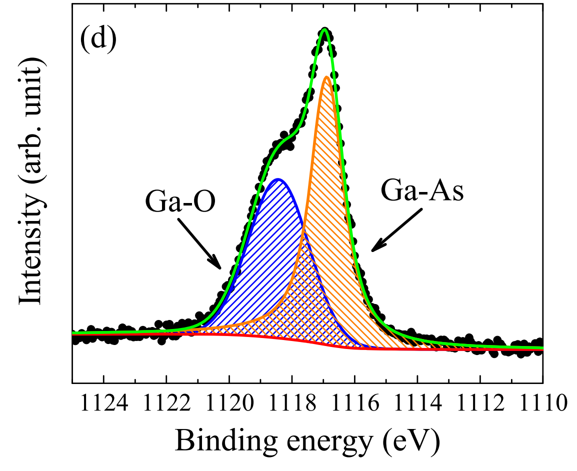

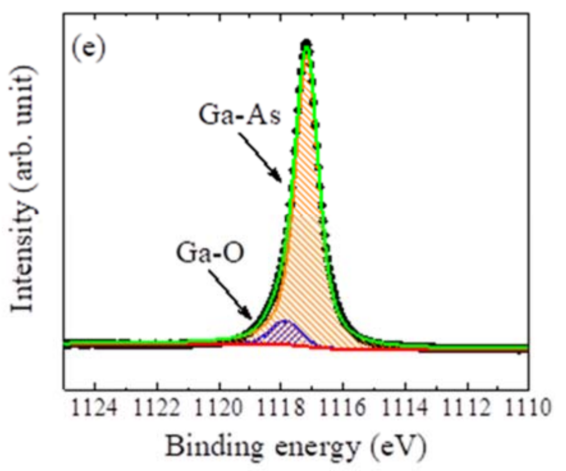

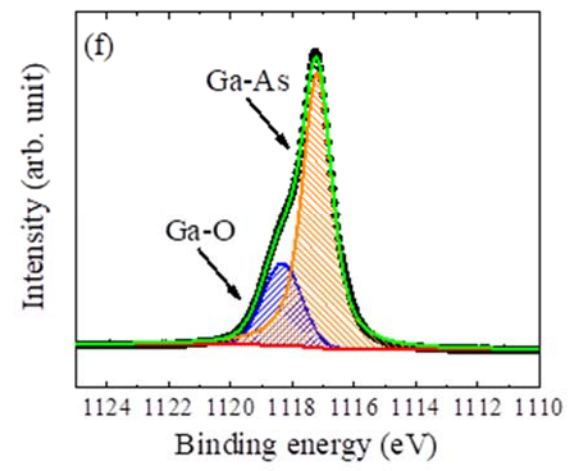

Fig. 2(a), (b), (c), (d), (e), and (f).

1
2
3
4
5
6
7
8
9
10
11
12
13
14
15
16
17
18
19
20
21
22
23
24
25
26
27
28
29
30
31
32
33
34
35
36
37
38
39

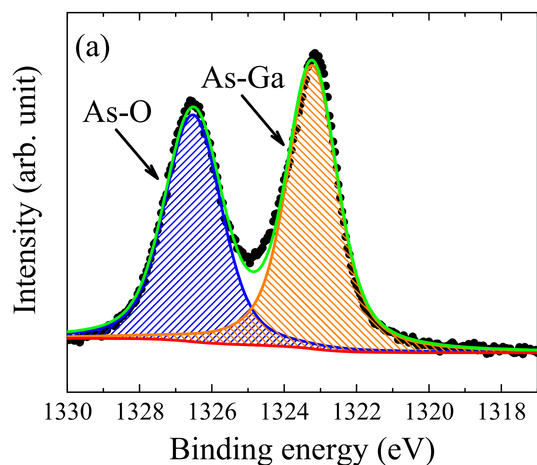

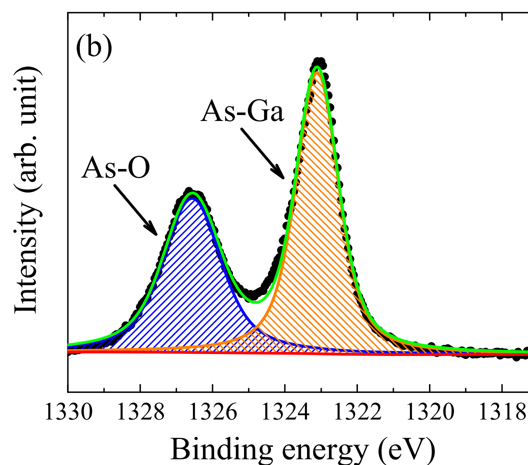

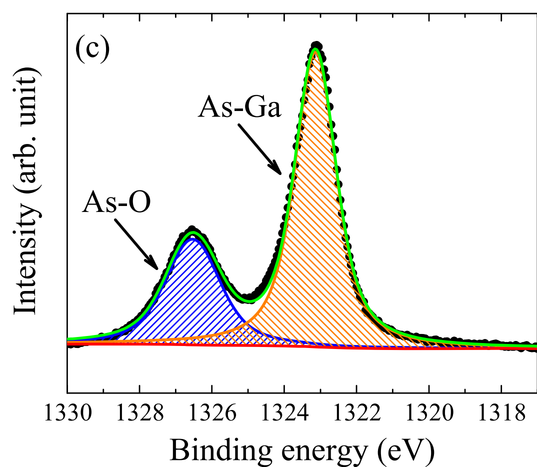

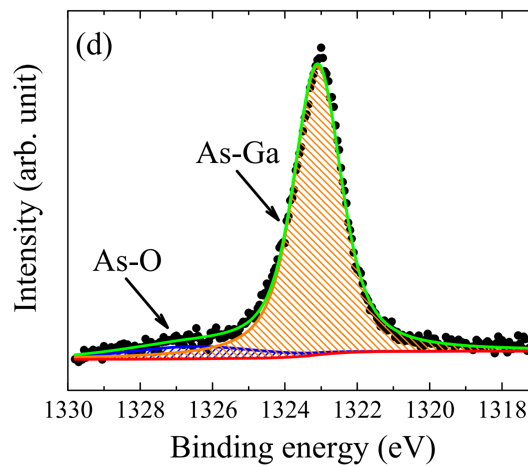

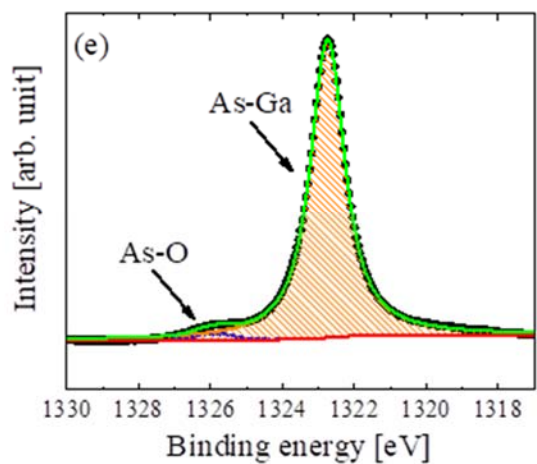

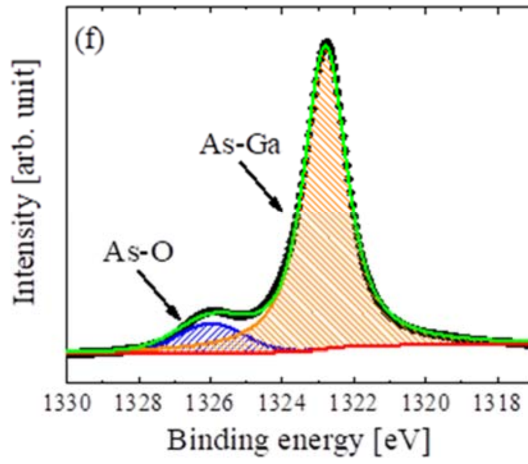

Fig. 3(a), (b), (c), (d), (e), and (f).

1

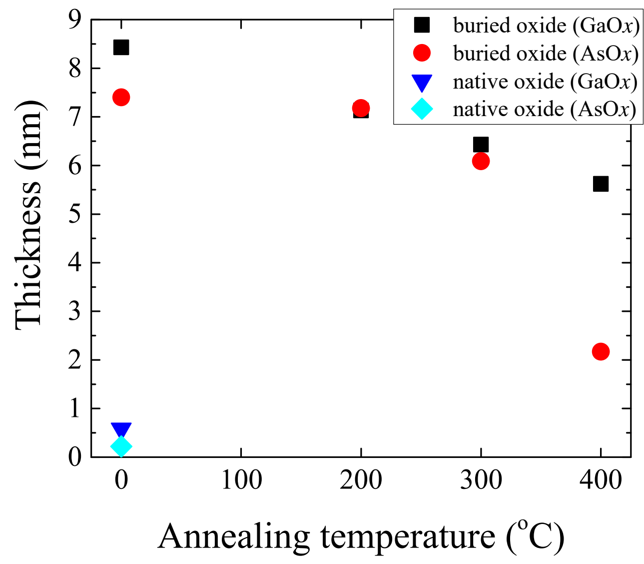

2

3

4

5 Fig. 4.

6

7

sample	**Binding energy FWHM**				**Normalized intensity**	
	Ga-As (eV)	Ga-O (eV)	As-Ga (eV)	As-O (eV)	Ga-O/Ga-As	As-O/As-Ga
GaAs sub. (unprocessed)	1117.1 0.9	1117.8 1.1	1322.7 1.1	1325.8 1.2	0.07	0.01
GaAs sub. (irradiated by Ar)	1117.1 1.1	1118.3 1.4	1322.8 1.4	1325.9 2.1	0.29	0.10
GaAs/Si (before annealing)	1117.3 1.2	1118.8 1.6	1323.2 1.6	1326.5 1.8	3.94	0.83
GaAs/Si (annealed at 200 °C)	1117.3 1.2	1118.8 1.6	1323.1 1.4	1326.5 1.9	1.49	0.74
GaAs/Si (annealed at 300 °C)	1117.4 1.2	1118.9 1.7	1323.1 1.3	1326.5 1.8	1.06	0.44
GaAs/Si (annealed at 400 °C)	1116.8 1.2	1118.4 2.2	1323.1 1.5	1326.5 4.3	0.75	0.09

Table I.